Knudsen pump inspired by Crookes radiometer with a specular wall

Tobias Baier* and Steffen Hardt
Center of Smart Interfaces, Institute for Nano- and Microfluidics, Technische Universität Darmstadt, 64287 Darmstadt, Germany

Vahid Shahabi and Ehsan Roohi
High Performance Computing Laboratory, Department of Mechanical Engineering, Ferdowsi University of Mashhad, 91775-1111 Mashhad, Iran
(Received 26 October 2016; published 22 March 2017)

A rarefied gas is considered in a channel consisting of two infinite parallel plates between which an evenly spaced array of smaller plates is arranged normal to the channel direction. Each of these smaller plates is assumed to possess one ideally specularly reflective and one ideally diffusively reflective side. When the temperature of the small plates differs from the temperature of the sidewalls of the channel, these boundary conditions result in a temperature profile around the edges of each small plate that breaks the reflection symmetry along the channel direction. This in turn results in a force on each plate and a net gas flow along the channel. The situation is analyzed numerically using the direct simulation Monte Carlo method and compared with analytical results where available. The influence of the ideally specularly reflective wall is assessed by comparing with simulations using a finite accommodation coefficient at the corresponding wall. The configuration bears some similarity to a Crookes radiometer, where a nonsymmetric temperature profile at the radiometer vanes is generated by different temperatures on each side of the vane, resulting in a motion of the rotor. The described principle may find applications in pumping gas on small scales driven by temperature gradients.

DOI: 10.1103/PhysRevFluids.2.033401

I. INTRODUCTION

The objective of this paper is to demonstrate and clarify some aspects of thermally induced gas flows beyond the continuum regime when the temperature profile is shaped essentially by wall segments with high specular reflectivity. This refers to situations where the mean free path ℓ of the gas molecules becomes comparable to or larger than a characteristic length scale W of the geometry, such as the width of a channel or the diameter of an object placed in the gas. The Knudsen number $\mathrm{Kn} = \ell/W$ thus becomes a suitable measure of the rarefaction of the gas. Deviations from the continuum regime start to become important at $\mathrm{Kn} \gtrsim 0.01$ such that the Navier-Stokes-Fourier set of transport equations has to be supplemented by temperature-jump and velocity-slip boundary conditions [1,2] within the slip flow regime ($0.01 \lesssim \mathrm{Kn} \lesssim 0.1$) or replaced by an alternative description such as the Boltzmann equation [2–4], in particular within the transition flow regime ($0.1 \lesssim \mathrm{Kn} \lesssim 10$) and the collisionless or free molecular regime ($\mathrm{Kn} \gtrsim 10$). When a nonhomogeneous temperature field is present in the gas, usually imposed by boundary conditions at walls, a gas flow can be induced, accompanied by forces on the boundaries. Classic examples are the thermophoresis of particles in a temperature gradient [5,6], the Crookes radiometer [7–9], and thermal transpiration through a porous material with an applied temperature gradient [8,10]. To this day these phenomena have not lost their attraction and inspire new implementations utilizing similar setups, as well as providing theoretical insight into thermally driven gas flows.

*baier@nmf.tu-darmstadt.de

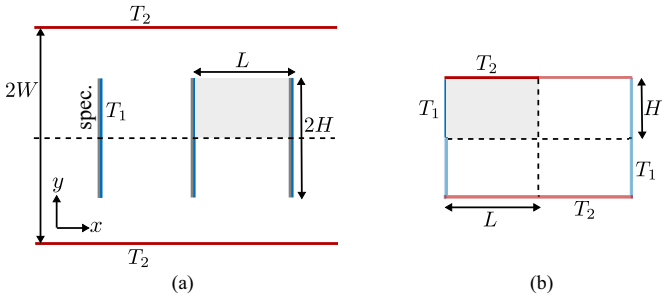

FIG. 1. (a) Sketch of the geometry. Vanes of height $2H$ are arranged with a spacing of L within a channel of width $2W$. The channel walls are diffusely reflecting and held at temperature T_2. The left sides of the vanes are specularly reflecting while their right sides are diffusely reflecting with temperature T_1. (b) Simplified geometry for the force calculation at $\mathrm{Kn} = \infty$ in Sec. II.

One example is the development of Knudsen pumps or compressors, which have received renewed interest with the advent of micromechanical systems and the associated microfabrication technologies. Optimal performance of these devices is typically reached somewhere between the slip and transition flow regimes such that reduced length scales allow operating them at atmospheric conditions. At such small scales Knudsen pumps are particularly appealing due to their lack of moving parts, since the gas actuation is due to thermal gradients along a channel with gas flowing from a colder to a warmer region. Practically implementable designs can be accomplished based on a periodic temperature profile along the walls of a channel [11–13] or by inducing thermal edge flow at an array of heated plates stacked within a channel [14]. An alternative implementation was recently proposed by Donkov *et al.* [15], where the gas flow is induced between surfaces held at different temperatures. Here one of the surfaces is considered to be structured in a ratchet pattern, with the inclined face of the ratchet reflecting gas molecules specularly, while the rest of the boundary reflects diffusely. A similar implementation relying on a purely diffusely reflecting ratchet geometry was proposed by Würger [16] and analyzed further in [17–19].

Over the years the Crookes radiometer, often referred to as a light mill, has served mainly as a demonstration object and as a testing ground for the theoretical understanding of rarefied gas flow in its different regimes of Knudsen numbers. After its discovery and the initial proposal for its operating principle by Reynolds [8] and Maxwell [9], it received a flurry of attention both experimentally and theoretically in the 1920s, mostly within the German literature put forward by the likes of Westphal [20], Einstein [21], Hettner [22], Sexl [23], Epstein [24], and Knudsen [25]. See [26] for an overview. In this period the close relation between the Crookes radiometer and thermophoresis of particles was pointed out [21,23,24] and we will later review these arguments inasmuch they pertain to the situation considered here. Similarly, the close relation between thermal transpiration in Knudsen pumps and the Crookes radiometer was already pointed out by Reynolds [8] and has recently led to alternative forms of the light mill [27,28]. Conversely, Taguchi and Aoki [29] considered the situation where vanes similar to the ones of a light mill are stacked in a channel with their planes normal to the channel direction. When one side of each vane is heated, for example, by illumination as in Crookes' original design, a gas flow around the edge of the vane is induced such that holding the vanes fixed leads to a net gas flow along the channel.

In most studies walls are considered as diffusely reflecting and temperature gradients are imposed by walls of different temperatures in close proximity, as in the case of the Crookes radiometer with vanes having a hot and a cold side. A wall where a significant part of the impinging gas molecules does not thermalize is often considered detrimental for the operation. In this paper we investigate a situation where temperature gradients are influenced by the presence of specularly reflecting walls in an essential way. Specifically, we consider the situation sketched in Fig. 1(a), where a series of vanes is placed inside a channel, similar to the geometry discussed by Taguchi and Aoki [29]. Here,

however, one side of each vane is considered to be ideally specularly reflecting and a temperature difference between the diffusely reflecting side of the vane, held at temperature T_1, and the sidewall of the channel, at temperature T_2, is imposed. We will consider the vanes as fixed, thus studying the setup as a Knudsen pump. However, a similarly operated Crookes radiometer is conceivable as well. Indeed, experimentally, the force on a Crookes radiometer is often quantified by operating it as a torsion balance, with the vanes suspended on a thread and measuring the deflection in a stationary state.

At first sight, studying specular surfaces may seem artificial, since it has been found experimentally that diffuse reflection represents a reasonable approximation for many surfaces, corresponding to tangential momentum accommodation coefficients not too far away from 1. However, there is clear experimental evidence that special surfaces expose accommodation coefficients much smaller than 1. For example, values between 0.1 and 0.4 have been recently reported [30–37]. Therefore, the scenario considered in this paper is certainly not a standard case in terms of molecule-wall interactions, but refers to pumping principles that could become feasible with special tailor-made materials. In order to assess the influence of the ideally specularly reflective wall we will compare with simulations based on a finite accommodation coefficient at the corresponding wall.

In the following we start by considering in Sec. II the proposed Knudsen pump with mixed specular and diffuse walls in the collisionless regime. Here exact expressions for the forces on all boundaries can be obtained. These serve as validation of and for comparison with the numerical results obtained via the direct simulation Monte Carlo (DSMC) method in Sec. III, spanning the slip flow and transition flow regimes. In Sec. IV the results for the normal force on the vanes are qualitatively explained along the lines of an argument put forward by Einstein, extended to the range of Knudsen numbers considered. Section V is dedicated to the velocity field and mass transport along the channel. Additionally, the ideal condition of vanishing accommodation on one vane face is relaxed. We close with a summary in Sec. VI.

II. COLLISIONLESS REGIME

To start with, we consider the collisionless regime, since here an analytical expression can be obtained for the force on the upper or lower wall and vanes, respectively. The force calculation proceeds along the lines of Donkov *et al.* [15]. The force density at position $\mathbf{r}_s$ on a wall is

$$\mathcal{F}(\mathbf{r}_s) = -\int m\mathbf{c}(\mathbf{c}\cdot\mathbf{n})f(\mathbf{r}_s,\mathbf{c})d^3c, \tag{1}$$

where the integral is over all values of $\mathbf{c}\in\mathbb{R}^3$ and $\mathbf{n}$ is the unit normal on the wall, pointing into the gas phase. The phase space density for particles leaving a diffuse wall, i.e., when $\mathbf{n}\cdot\mathbf{c} > 0$, is $f(\mathbf{r}_s,\mathbf{c}) = n(\beta/\pi)^{3/2}e^{-\beta\mathbf{c}^2}$, where $\beta = m/2k_BT$ is determined by the temperature T of the wall and the particle number density $n = 2\sqrt{\pi\beta}\nu$ is determined by the particle flux density ν (number of molecules impinging per unit time and unit area on the surface) as well as the temperature of the diffuse wall. Note that in the collisionless regime ν is constant on all walls (see Ref. [2], Sec. 2.5.1, or Ref. [38]). At a specular wall, the phase space density obeys the symmetry relation $f(\mathbf{r}_s,\mathbf{c}) = f(\mathbf{r}_s,\mathbf{c}-2\mathbf{c}\cdot\mathbf{n})$, directly linking the distributions for impinging and reflected particles. The phase space density for particles impinging at $\mathbf{r}_s$ is obtained by tracing backward along the particle trajectories, if necessary taking into account specular reflections, until a diffuse wall with a known phase space distribution is reached.

With these prerequisites, the average force density on the upper wall can be calculated; owing to the mirror symmetry of the model, the force density on the lower wall is obtained by mirror reflection. The calculation is simplified by noting that from the vantage point of any position within the gray area in Fig. 1(a) the upper diffuse wall looks completely homogeneous, since all particles originating from this wall have the same phase space distribution irrespective of the viewing angle. Thus the particle number, momentum, or energy fluxes entering the gray area from above will be the same irrespective of the distance of the top wall from the vanes. The same is obviously also true for

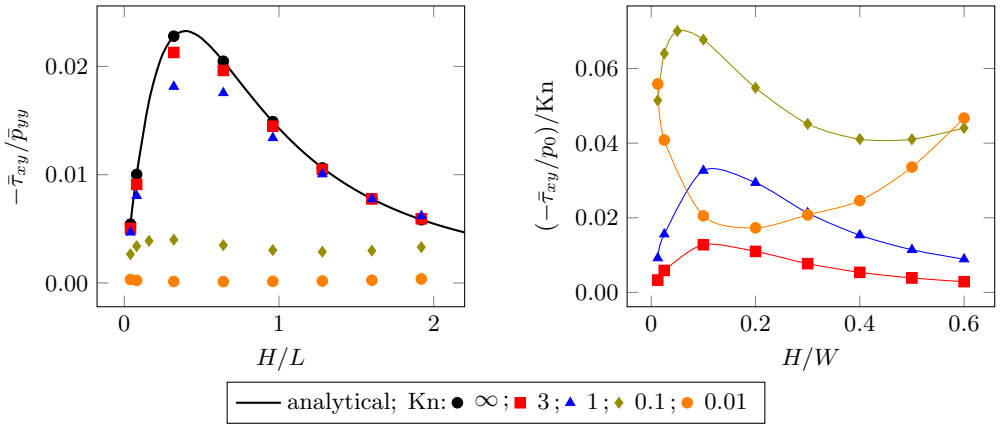

FIG. 2. Shown on the left is the ratio of the average tangential and normal stresses on the sidewall of the channel $\bar{\tau}_{xy}/\bar{p}_{yy}$ as a function of H/L for $T_2 = 2T_1$ and $W/L = 3.2$. The solid line show the analytical result in the collisionless regime and the symbols the DSMC results for $\mathrm{Kn} = 0.01$, 0.1, 1, 3, and ∞. On the right are the same tangential stress data as on the left but using the pressure scale $\hat{p}_0 = p_0\mathrm{Kn}$ for normalization, as discussed in the text (lines are merely guides for the eye).

the fluxes leaving the gray area towards the top wall. Therefore, the analysis can be performed in the special case where $W = H$ such that only a single unit cell has to be considered. This is illustrated in Fig. 1(b), where the gray area of Fig. 1(a) corresponds to the respective region in the upper left quadrant. By symmetry at the channel centerline and due to the specular side of the vane, illustrated by the horizontal and vertical dotted lines, respectively, we can extend the region of interest to one bounded by diffuse walls only, where consequently the phase space density of the outgoing particles is known. The mean momentum flux towards and away from the upper wall can thus be obtained by averaging the local force density (1) on the original section of this wall bounding the gray area. In particular, the average tangential force per area on the upper wall is

$$\bar{\tau}_{xy} = \frac{\sqrt{\pi}}{2} \nu m (\bar{c}_2 - \bar{c}_1) \frac{H}{L} \left[\frac{2}{\pi} \left(\arctan \frac{L}{H} - 2 \arctan \frac{L}{2H} \right) \right], \tag{2}$$

where we have introduced the characteristic velocity $\bar{c}_i = 1/\sqrt{\beta_i} = \sqrt{2k_B T_i/m}$ of diffusely reflected molecules from a wall at temperature T_i. The limiting values for the expression in square brackets are 0 and -1 for $L/H \to 0$ and ∞, respectively, and the values remain within these limits for intermediary values of L/H. The tangential force density vanishes for $L/H \to 0$ and ∞ and becomes extremal at $L/H \approx 2.62$. We note that, due to conservation of momentum, a force of equal magnitude opposite to that on the sidewalls must act on the vanes such that the corresponding average force density on a vane in the x direction is $\bar{\mathcal{F}}_x|_{\mathrm{vane}} = -(L/H)\bar{\tau}_{xy}|_{\mathrm{side}}$.

Similarly, the average normal force per area on the upper wall is

$$\bar{p}_{yy} = \frac{\sqrt{\pi}}{2} \nu m \left((\bar{c}_2 + \bar{c}_1) + (\bar{c}_2 - \bar{c}_1) \left[\frac{2}{\pi} \arctan \frac{L}{H} \right] \right). \tag{3}$$

The limiting values for the expression in square brackets are 0 and 1 for $L/H \to 0$ and ∞, respectively.

The ratio between tangential and normal forces is independent of the particle flux density ν as well as the particle mass and becomes solely a function of the geometrical parameters and the wall temperatures. As shown by the solid line on the left panel of Fig. 2, the force ratio vanishes for large and small values of H/L with an extremum at $H/L \approx 0.4$. In the next section we compare this result with numerical values obtained for finite Knudsen numbers. Since the net gas velocity vanishes identically in the collisionless regime [2], obviously no mass transport takes place along

the channel in this situation. Nevertheless, it is plausible that the net transfer of momentum in the channel direction from the vanes to the walls results in a corresponding net mass flux as collisions between molecules become more prominent.

III. FINITE KNUDSEN NUMBERS

The DSMC method [39] is a particle-based scheme for solving the Boltzmann equation for the phase space density in a rarefied gas, where particle collisions are introduced probabilistically. We use an implementation of the method in dsmcFoamStrath [40–42] within the framework of openFOAM [43], version 2.3.x, relying on its capabilities of Lagrangian particle tracking. The simulation domain is one unit cell in Fig. 1(a) with $W/L = 3.2$ and variable H/L. The vane is located in the middle of each unit cell that has cyclic boundary conditions at the left and right sides and a symmetry boundary condition at the bottom, representing the channel centerline. This domain is discretized into 100×300 sample cells and the simulations are initialized such that on average 40 DSMC particles are located within each cell. During the simulation, each of the cells is locally adapted to collision subcells using the transient adaptive subcell feature of the dsmcFoamStrath solver, in a manner that the number of subcells depends on the local cell's number density [44]. The time step Δt is chosen such that $\ell/\bar{c}_1\Delta t \geqslant 10$ (except for $\mathrm{Kn} = 0.005$, where $\ell/\bar{c}_1\Delta t = 5$). Each configuration was run for at least 10^6 time steps, where typically more time steps were allotted to runs with lower Kn.

For all simulations we assume that the temperature of the sidewalls is twice the temperature of the vanes $T_2 = 2T_1$, where the temperature scale was set to $T_1 = 300$ K. We define the Knudsen number as $\mathrm{Kn} = \ell/W$, where the mean free path $\ell = (\sqrt{2}n_0\pi d^2)^{-1}$ depends on the particle diameter and the mean particle number density n_0. For the DSMC simulations the variable hard sphere binary collision model with the Larsen-Borgnakke model for rotational internal energy redistribution [45] is used to model collisions between molecules. We assume nitrogen with a diameter of $d = 4.17 \times 10^{-10}$ m, a viscosity temperature index of $\omega = 0.74$, a reference temperature of $T_{\mathrm{ref}} = 273$ K, and a mass of $m = 46.5 \times 10^{-27}$ kg.

We use the usual definitions of the particle number density $n(\mathbf{r}) = \int f(\mathbf{r},\mathbf{c})d^3c$, the velocity $\mathbf{u}(\mathbf{r}) = [n(\mathbf{r})]^{-1}\int \mathbf{c}f(\mathbf{r},\mathbf{c})d^3c$, and the pressure tensor $p_{ij}(\mathbf{r}) = m\int (\mathbf{c}-\mathbf{u})_i(\mathbf{c}-\mathbf{u})_j f(\mathbf{r},\mathbf{c})d^3c$, which is split into a diagonal and a traceless part via $p_{ij}(\mathbf{r}) = p(\mathbf{r})\delta_{ij} + \tau_{ij}(\mathbf{r})$, with the pressure $p(\mathbf{r}) = (1/3)\sum_i p_{ii}(\mathbf{r})$ and the shear stress tensor $\tau_{ij}(\mathbf{r})$. The temperature obeys the ideal gas equation of state $p(\mathbf{r}) = n(\mathbf{r})k_B T(\mathbf{r})$, where k_B is the Boltzmann constant. The net mass flow along the channel is the integral $\dot{m} = m\int n(\mathbf{r})u_x(\mathbf{r})dA$ over the cross section of the channel. For normalization we introduce $T_0 \equiv T_1$ as the temperature scale and $\bar{c}_0 \equiv \bar{c}_1 = \sqrt{2k_B T_1/m}$ as the velocity scale, i.e., values based on the temperature at the vane. Similarly, we introduce the density scale n_0 as the average density corresponding to the respective Knudsen number. The corresponding pressure scale is $p_0 = n_0 k_B T_0$, used for normalizing the pressure and shear stress tensors. The mass flow along the channel is normalized with $\dot{m}_0 = Amn_0c_0$, where A is the full cross-sectional area of the channel. For integrated quantities such as the mass flow or area-averaged force densities, the numerical error is estimated as the standard deviation from at least three consecutive runs. For all such quantities presented in the figures within this work the error is smaller than the size of the symbols and thus no error bars are plotted.

The method is validated in the collisionless regime to assess its accuracy. The absolute value of the ratio of the tangential and normal force on the sidewall of the channel is shown in the left part of Fig. 2 for different values of H/L. Since $T_2 > T_1$, the force on the sidewalls is towards the left [see Eq. (2)]. Correspondingly, the force on the vanes is towards the right in this situation. As can be seen, the agreement between the DSMC and analytical results is excellent. For decreasing Kn, the ratio of tangential and normal force decreases, but the functional form with respect to H/L remains similar to the collisionless case up to $\mathrm{Kn} \approx 1$. Experiments are conveniently done in a fixed geometry by adjusting Kn via the gas pressure and this decrease in $\bar{\tau}_{xy}/\bar{p}_{yy}$ is largely due to the increased pressure for small values of the mean free path. To directly compare forces measured at different

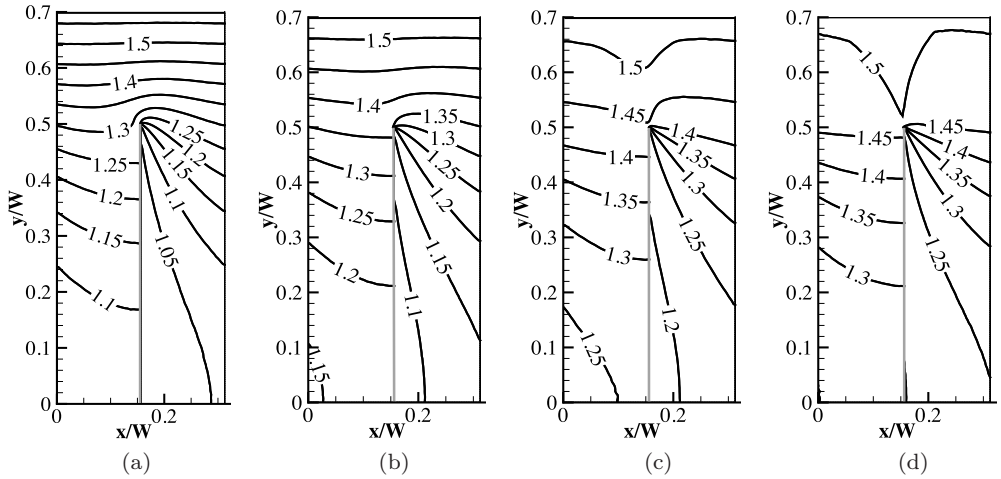

FIG. 3. Isolines of temperature T/T_0 for (a) Kn $= 0.01$, (b) Kn $= 0.1$, (c) Kn $= 1$, and (d) Kn $= 3$ ($H/W = 0.5$ and $H/L = 1.6$).

Kn in such an experiment it is thus preferable to use a reference pressure that is independent of Kn. This is illustrated in the right panel of Fig. 2, where the pressure $\hat{p}_0 = p_0\,\mathrm{Kn}$ is used as a reference scale. As can be seen, within the transition flow regime down to Kn $\lesssim 0.1$, the tangential force on the sidewall increases with increasing pressure. Its form as a function of H/W also changes from its single maximum at large Kn, attained for relatively small vanes. For smaller Kn, this maximum appears to migrate towards smaller values of H/W, while a secondary maximum appears for vanes occupying a large part of the channel due to an increased temperature gradient between the vane and sidewall, as the intermediary gap shrinks with increasing H/W.

Before delving further into the dependence of the force on Kn, we show isolines of temperature and pressure as well as streamlines in Figs. 3, 4, and 8 for $H/W = 0.5$ and $H/L = 1.6$ at various Kn. In Fig. 3 we observe that the pattern of temperature isolines at the tip of the vane is not radically different for the different Knudsen numbers. It is apparent, however, that the temperature gradient at

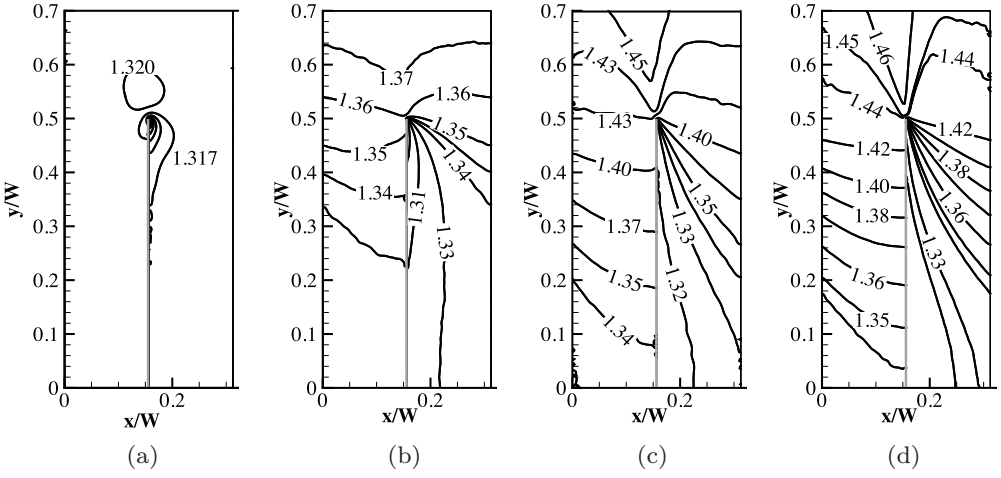

FIG. 4. Isolines of pressure p/p_0 for (a) Kn $= 0.01$, (b) Kn $= 0.1$, (c) Kn $= 1$, and (d) Kn $= 3$ ($H/W = 0.5$ and $H/L = 1.6$).

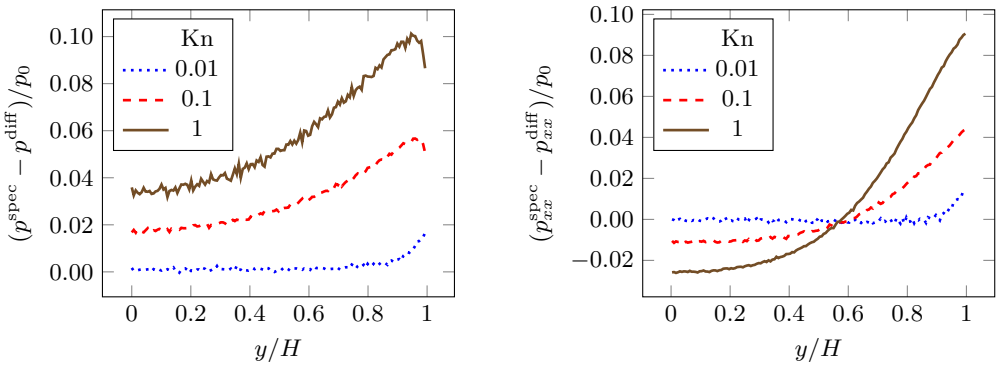

FIG. 5. Shown on the left is the normalized pressure difference across the vane as a function of distance from the centerline for Kn = 0.01, 0.1, and 1. On the right is the normalized difference in p_{xx} across the vane (i.e., net force density in the x direction on the vane) as a function of distance from the centerline ($H/W = 0.5$ and $H/L = 1.6$).

the tip of the vane becomes more and more pronounced for smaller Knudsen numbers. Of course one has to keep in mind that particularly for Kn > 1 the phase space distribution function is very different from an isotropic Maxwell distribution described by the scalar quantities density and temperature, but has a strong direction dependence in the velocity. For all Knudsen numbers shown, this is also reflected in the temperature jump between a diffuse wall and the adjacent gas, which becomes larger with increasing mean free path.

The pressure distribution p/p_0 around the vane is shown in Fig. 4. At large Kn, the isobars follow roughly the same pattern as the isotherms. At Kn $\lesssim 0.1$, however, some isobars originating from the tip of the vane curve back onto the diffuse side of the vane and for lower Kn only the pressure in a small region extending a few mean free paths around the tip of the vane differs appreciably from its average value in the surroundings. This is an indication that for small Kn the main contribution to the net force is concentrated at the tip, extending only a few mean free paths along the vane. Note that the force on the vane is given by the integral of p_{xx} along the vane. Due to the temperature gradient across the vane, the pressure tensor p_{ij} is not isotropic, such that $p_{xx} \neq p_{yy}$. Therefore, p is not the only contribution to the force on the vane. This is investigated in Fig. 5, where the difference in p (left) and p_{xx} (right) between both sides of the vane is plotted as a function of the position along the vane. As can be seen, even for Kn as small as 0.1, the net force density does not vanish at the center of the vane and in this particular geometry also changes its sign such that the gas pushes towards the left at the center of the vane and to the right towards its edges. Only for smaller Kn, to a good approximation, the net force density indeed vanishes everywhere except at the tip. Since the Knudsen number Kn $= \ell/W$ is based on the channel width, we have $\ell/H = 0.02$ at Kn $= 0.01$ and $W = 2H$ such that the width of the edge zone is roughly 5ℓ in this case.

In the left panel of Fig. 6 we plot the normalized mean shear stress $-\bar{\tau}_{xy}/p_0$ on the channel walls as a function of Kn. We remind the reader that, due to momentum conservation, the mean force per unit area on the vane is $\bar{\mathcal{F}}_x|_{\mathrm{vane}} = -(L/H)\bar{\tau}_{xy}|_{\mathrm{side}}$. Evidently, $\bar{\tau}_{xy}/p_0$ tends to a constant for large Kn, while for small Kn it scales as $\sim \mathrm{Kn}^{1.5}$. Since in a typical experiment Kn is varied by changing the pressure $p_0 \sim \mathrm{Kn}^{-1}$, the force density on the vane thus scales as $\bar{\mathcal{F}}_x \sim \mathrm{Kn}^{0.5}$ for small Kn and $\sim \mathrm{Kn}^{-1}$ for large Kn and becomes extremal for Kn between 0.01 and 0.1. This is illustrated in Fig. 6 on the right, where we again use the reference pressure $\hat{p}_0 = p_0\mathrm{Kn}$. Note that this scaling of the force with Kn agrees with results obtained for purely diffuse plates with sides held at different temperatures [46,47].

Before turning to the performance of the setup as a pump, we give a qualitative explanation for the magnitude of the force as a function of Kn in the next section.

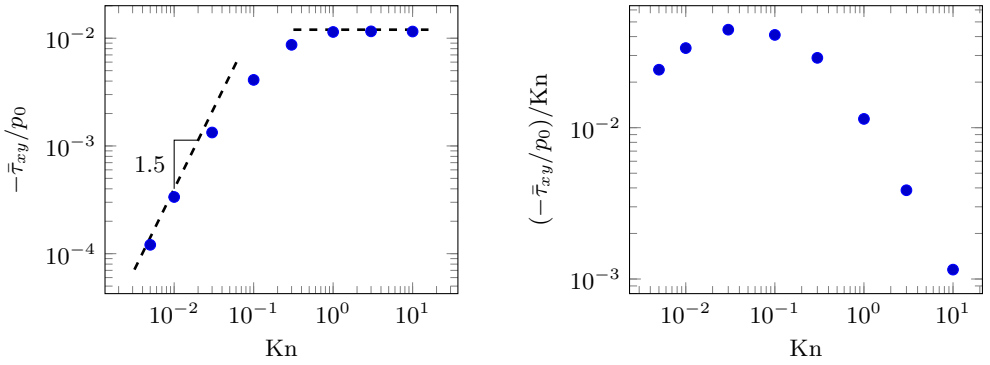

FIG. 6. Shown on the left is the normalized force density $\bar{\tau}_{xy}/p_0$ on the channel sidewall as a function of Kn at $H/W = 0.5$ and $H/L = 1.6$. On the right are the same data as on the left but using the pressure scale $\hat{p}_0 = p_0\mathrm{Kn}$ for normalization, as discussed in the text.

IV. SCALING ANALYSIS

In Fig. 3 we saw that the specular-diffuse plate introduces a strongly asymmetric temperature profile around the edge of the vane that leads to a net normal stress on the vane. To discuss such normal stresses on an object in a temperature gradient in rarefied gases, we consider a simplified geometry shown in Fig. 7, where a small plate is located midway between two plates of infinite extent at different temperatures. Although not strictly necessary for the argument, consider for the moment the case where the small plate's temperature is midway between the temperatures of the two plates and that the plate's sides are either purely diffusely or specularly reflecting. Due to the temperature gradient over the plate, on average the right side is hit by slightly faster molecules than the left side. The incoming gas molecules thus impart a net momentum in the $-x$ direction onto the plate from the hotter to the colder side. Similarly, unless both sides of the plate are diffusely reflecting at the same temperature, on average the reflected particles contribute a normal force on the plate that is again larger on the hotter side. By momentum conservation, an opposite force of equal magnitude is imparted onto the reflected gas molecules by the plate. Note that without the small plate, the gas phase would be at rest.

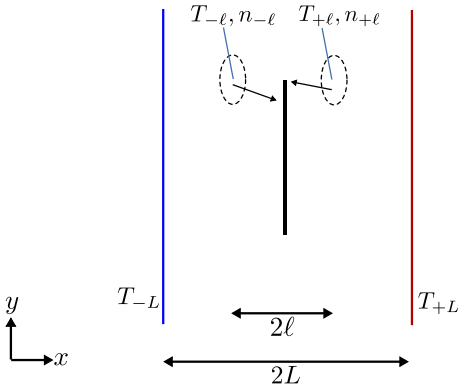

FIG. 7. Sketch of a plate inserted in the space between two plates at temperatures T_{-L} and T_{+L}, respectively. For $T_{-L} < T_{+L}$, due to the net heat flux towards the left, molecules impinging onto the plate from the right carry a larger momentum than molecules from the left, leading to a net force on the plate towards the left normal to the face of the plate. If the plate is stationary, a corresponding gas flow around the plate edges towards the right is induced (from cold to hot).

The magnitude of this force can be estimated as follows, loosely following an argument by Einstein [21]. Molecules arriving from the right and left sides of the plate will have a characteristic molecular velocity along the x axis $\bar{c}_{\pm\ell} = \sqrt{2k_B T_{\pm\ell}/m}$ depending on the temperature at the position one mean free path away from the plate, as indicated by the corresponding subscript and sketched in Fig. 7. For situations where the gas velocity is much smaller than the characteristic molecular velocity, i.e., low Mach number, the molecular flux of particles from the right towards the edge of the plate is thus approximately $\frac{1}{2}n_{+\ell}\bar{c}_{+\ell}$, where $n_{+\ell}$ is the number density one mean free path to the right of the edge and we have assumed that half of the particles originating from that position move to the left with a characteristic velocity $\bar{c}_{+\ell}$ in the x direction. If no plate were present, this flux must be compensated by a corresponding flux $\frac{1}{2}n_{-\ell}\bar{c}_{-\ell}$ of molecules from the left and we assume this relation to hold approximately also at the edge of the plate, at least within a region of size ℓ. Therefore, $n_{+\ell}\bar{c}_{+\ell} \approx n_{-\ell}\bar{c}_{-\ell}$, which we abbreviate as $n\bar{c}$. The corresponding flux of x momentum carried in the x direction by these particles is thus $(\frac{1}{2}n_{\pm\ell}\bar{c}_{\pm\ell})(m\bar{c}_{\pm l}) \approx \frac{1}{2}n\bar{c}m\bar{c}_{\pm l}$. Since they hit opposite sides of the plate they impart a net force per unit area of

$$\mathcal{F}_{\mathrm{E}} \approx \tfrac{1}{2}nm\bar{c}(\bar{c}_- - \bar{c}_+) \approx -nm\bar{c}\ell\partial_x\bar{c} \approx -k_B n\ell\partial_x T \approx -(p/T)\ell\partial_x T \tag{4}$$

on the plate in the x direction, where $\bar{c} = \sqrt{2k_B T/m}$ was used to convert between the molecular velocity scale and the temperature. We stress that the derivative should be regarded as shorthand for the normalized difference of properties approximately one mean free path to the left and right of the plate.

Apart from a factor of $\frac{1}{2}$, Eq. (4) agrees with Einstein's estimate. Of course the total force on the plate is governed by the momentum flux of particles both impinging on and reflected from the surface. However, when both sides of the plate reflect diffusely at the same temperature the contributions of the reflected particles on both sides of the plate cancel (since the particle flux is equal) and for a purely specularly reflecting plate the reflected particles contribute with a magnitude equal to that of the impinging ones, since the normal component of the velocity of the impinging particles is reversed.

We thus stress that irrespective of the boundary condition at the wall, there is a normal force on the plate as long as there is a temperature gradient normal to the plate. The boundary condition on the plate itself may be the origin of this temperature gradient, for example, when the accommodation coefficient or wall temperature differs on opposite sides of the plate. However, the temperature gradient is usually also affected by the boundary conditions far away from the plate. Furthermore, the accommodation coefficient influences the magnitude of the force via the momentum transferred by the recoil of the reflected molecules.

Equation (4) is an estimate of the force density within a region extending a distance of ℓ away from the edge of the plate. To find the force on the plate we consider three different regimes depending on the Knudsen number. To begin, we start in a regime where the density is so low that the mean free path ℓ becomes comparable to the size of the container the plate is embedded in. In this case the thermal velocity of the gas molecules is essentially governed by the temperature of the last diffuse wall (container boundary or plate) from which these molecules scatter. An appropriate estimate of the force density is obtained by replacing $\ell\partial_x T$ in Eq. (4) with the temperature difference ΔT between the plate and the corresponding wall. The force is obtained by multiplying the force density with the plate area d^2 such that $F \sim -d^2 n k_B \Delta T$, which in particular scales as $\sim n$ for small gas densities. Since the product $n\ell$ is a constant, this means that $F \sim \mathrm{Kn}^{-1}$ in this regime. This can be considered as the free molecular regime discussed in Sec. II.

Next consider a regime where ℓ is larger than the plate dimension d but smaller than the container dimension. In this case the temperature field in the gas is governed by continuum-scale convective-diffusive heat transport, apart from a region a distance $\sim\ell$ away from the walls, and (4) is an adequate approximation on the entire plate surface. Thus $F \sim -d^2 k_B n\ell\partial_x T$, which, since $n\ell$ is constant, is a regime where the force is approximately independent of the Knudsen number. This is essentially the regime considered for thermophoresis of small particles [21,48,49].

Finally, when the mean free path ℓ becomes much smaller than the plate dimensions, we have to consider the fact that (4) is only valid at the edge of the plate. Unless the external setup is such that the system works as a pump, the pressures on both sides of the plate are equal and viscous or thermal stresses in the gas are negligible away from the edges of the plate. Since only a region of the extension of the mean free path around the edge contributes, the force on the plate scales as $F \sim -dk_B n\ell^2 \partial_x T$. In this regime, the force is thus expected to scale with $\ell \partial_x T$. This is the regime considered for radiometer forces by Einstein. For constant $\partial_x T$ the force scales like $F \sim n\ell^2 \sim \mathrm{Kn}$ in this regime. However, while (4) can be rigorously corroborated for large and intermediate Kn as long as the molecular velocity distribution is dominated by boundary conditions far away from the plate, for low Kn the temperature profile may be strongly influenced by the presence of the plate. Similar to the scaling of thermal edge flow at the edge of a heated plate found by Sone and Yoshimoto [50], one often finds a dependence closer to $\ell \partial_x T \sim \mathrm{Kn}^{1/2}$ within a region of size ℓ around the tip in the radiometer case as well and the corresponding force-scaling becomes $F \sim \mathrm{Kn}^{1/2}$ (see Ref. [46]). In the present case, an analogous scaling should be expected due to the similarity of the temperature field. Note that a similar scaling was employed by Wang *et al.* [19] in the context of thermally induced channel flow at the tips of ratchet teeth protruding into a channel.

In total, from the physical picture sketched above it can be inferred that the force on the plate has a maximum at an intermediate Kn and drops off at $\sim \mathrm{Kn}^{0.5}$ and $\sim \mathrm{Kn}^{-1}$ for smaller and larger Kn, respectively. This is indeed what is observed in the simulation results shown in Fig. 6, corroborating our reasoning.

The qualitative derivation of (4) is analogous to the explanation given for thermal creep flow along a wall with a tangential temperature gradient [2,51]. Here, again molecules impinging on the wall from a region of higher temperature impart a larger momentum than molecules originating from a colder region. In the case of a diffusely reflecting wall this leads to a net tangential force on the wall towards the colder region. Conversely, for a stationary wall a creep flow along the wall towards the warmer region is induced in the gas phase, described by the Maxwell slip boundary condition [2,52]. In the present case of specular-diffuse vanes in a channel, since the corresponding force density is tangential to the boundary, it does not directly contribute to the net force on the vanes in the channel direction, i.e., normal to the vanes. However, for a plate of finite thickness with a temperature gradient along its edge, this tangential force component can contribute directly to the force on the Crookes radiometer [22,53,54].

V. PUMPING PERFORMANCE

Since the gas exerts a net force in the x direction on the vanes, an equal but opposite force acts on the reflected gas molecules due to the interaction. At finite Kn this leads to a net flow of the gas phase, as shown in Fig. 8. Since the net force on the vane is towards the right, a net flow towards the left is induced in the gas. For Kn up to 0.1 the tip of the vane acts similarly to a localized volume force density in its vicinity, driving the gas towards the left such that the flow pattern resembles a Couette flow in the region between the vanes and the channel wall. As the mean free path becomes of the same order of magnitude as the channel dimension, the details of the flow field are expected to be significantly influenced by boundary conditions farther away and not solely by the local temperature field at the edge of the vane. Indeed, for $\mathrm{Kn} = 1$ the flow field can be seen to become qualitatively different from the Couette like flow for lower Kn, with a vortex emanating from the specular side of the vane reaching into the channel. This vortex grows with the mean free path and at $\mathrm{Kn} = 3$ eventually fills the whole region between the vanes and the sidewalls of the channel. This change in flow pattern has interesting consequences for the mass flow along the channel shown in Fig. 9 (left side). While for small Kn the flow is in negative the x direction, for large Kn a net flow in the opposite direction is observed.

The magnitude of the net mass flux in the continuum regime can be estimated on the basis of the discussion of the forces on the vanes and sidewalls in Sec. IV. Within a region of the size of

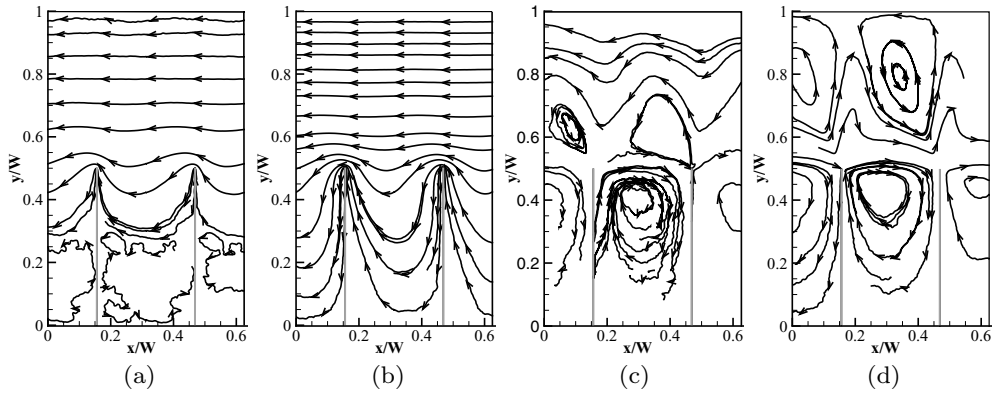

FIG. 8. Streamline patterns at (a) Kn = 0.01, (b) Kn = 0.1, (c) Kn = 1, and (d) Kn = 3 (for $H/W = 0.5$ and $H/L = 1.6$).

one mean free path around the edge, momentum is exchanged between the vane and gas. At low Kn the effect of this is similar to that of localized momentum sources at the edges of the vanes, while the Stokes equation governs the velocity within the rest of the domain, resulting in a velocity profile similar to Couette flow within the open section of the channel. The velocity is thus expected to scale as $\bar{u} \sim \tau h/\eta$, where τ is the shear rate at the side wall, h is a length scale of the order of the distance between the vane and side walls, and η is the mean viscosity. Since at moderate pressures the viscosity does not depend on pressure, the dependence of the velocity on Kn is the same as for the force on the vane and sidewall.

On the other extreme of very large Knudsen numbers, i.e., the collisionless regime, the gas velocity vanishes everywhere [2]. For large but finite Kn we can imagine the phase space distribution function $f = f_\infty + \delta f$ to become altered slightly relative to the collisionless distribution f_∞ by a few collisions between the gas molecules. Since the collision probability for each molecule is proportional to the gas density, the relative change in phase space distribution $\delta f/f_\infty$ and hence the mean gas velocity are expected to be proportional to the gas density, i.e., $\bar{u}/c_0 \sim \mathrm{Kn}^{-1}$ in this regime.

Overall, the nondimensionalized flow velocity and hence the nondimensionalized mass flux are thus expected to scale $\sim\mathrm{Kn}^{0.5}$ and $\sim\mathrm{Kn}^{-1}$ for small and large Kn, respectively. In order to capture

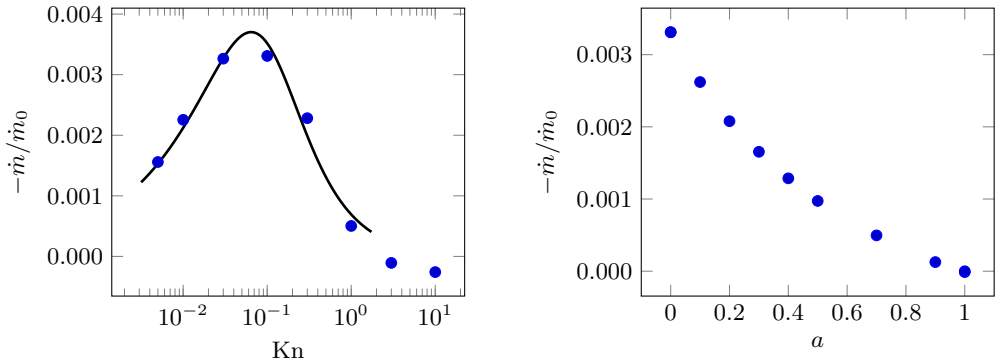

FIG. 9. Shown on the left is the normalized mass flow in the channel as a function of Kn. The solid line corresponds to a least-squares fit of $g(\mathrm{Kn}; a, b) = (a\,\mathrm{Kn}^{-0.5} + b\,\mathrm{Kn})^{-1}$ to the values for $\mathrm{Kn} \leqslant 1$ ($H/W = 0.5$ and $H/L = 1.6$). On the right is the normalized mass flow in the channel as a function of the accommodation coefficient a (Kn = 0.1, $H/W = 0.5$, and $H/L = 1.6$).

both limits, the function $g(\mathrm{Kn};a,b) = (a\,\mathrm{Kn}^{-0.5} + b\,\mathrm{Kn})^{-1}$ was used in a least-squares fit for the positive data points on the left panel in Fig. 9 and plotted as a solid line. As can be seen, the function captures the dependence on Kn very well, corroborating our argument. However, we stress again that this can only be a crude approximation and not too much importance should be assigned to the quality of this fit since, as we have seen in particular for $\mathrm{Kn} > 1$, the boundary conditions far away from the vane can lead to a qualitatively different flow field than at intermediate and small Kn. We briefly demonstrate this in Appendix A, where the flow pattern and net mass flow at large Kn for vanes occupying different fractions H/W of the channel are discussed. Additionally, we show that significantly larger flow rates can be obtained by reducing the vane size. As shown in the right panel of Fig. 12, in terms of an optimal geometry for a Knudsen pump, a vane of size $H/W = 0.1$ performs at a roughly 5 times higher flow rate at $\mathrm{Kn} = 0.1$ compared to the case $H/W = 0.5$ discussed so far.

So far we have considered the left sides of the vanes to be perfectly specularly reflective. In order to assess the impact of a departure from this idealized condition on the pumping performance, we relax this assumption and consider a situation where the left sides are characterized by a Maxwell-type boundary condition [2] with accommodation coefficient a between 0 (fully specular) and 1 (fully diffuse). For molecules reflected diffusely from these walls the temperature is set to T_1, as on the right side of the vanes. The normalized mass flow in this situation is plotted as a function of a on the right panel of Fig. 9. It is evident that even for a partially specular wall, substantial mass flows are observed. However, since our focus was expressly on the impact of walls of high specular reflectivity, we will not pursue this further here.

The pumping performance of the idealized pump studied here can be compared to other configurations described in the literature that are either geometrically similar or use a similar pumping mechanism for generating an inhomogeneous temperature profile along a channel. Although a direct comparison is difficult due to the different simulation parameters used in the studies, in particular with respect to the specific geometry and applied temperature range, a qualitative comparison is feasible, assuming linearity of the pumping performance with the temperature difference applied. In the geometrically similar configuration studied by Taguchi and Aoki [29] the temperature profile in the channel is generated by applying different temperatures on both sides of the vanes, considering fully diffuse reflection. In this setup, the mass flow is slightly larger than in the present configuration, but of the same order of magnitude. The better performance of this configuration most likely stems from the larger temperature gradients at the tips of the vanes due to directly prescribing the temperatures instead of indirectly generating a temperature profile via a specular boundary. Wang *et al.* [19] considered a channel with one flat diffusely reflecting wall and an opposing surface structured as a ratchet with parts of each ratchet tooth reflecting diffusely and parts fully specularly, similarly to the vanes considered here. The temperature profile in the channel is generated by prescribing different temperatures at the opposing walls. The mass flow obtained with this configuration is of the same order of magnitude as the one observed here. In a similar configuration, Chen *et al.* [18] used two opposing ratchet surfaces and considered several different reflection properties at the walls. In the situation where the opposing walls are fully diffusely reflecting, the mass flow rates obtained are one to two orders of magnitude smaller than in the present case. However, when using alternating diffuse and purely specular segments on each ratchet tooth, the mass flow rates obtained are again of the same order of magnitude as the ones in the present setup.

VI. CONCLUSION

Maxwell [9] proposed a simple model for the gas-surface interaction that is intermediate between diffuse reflection and specular reflection, with an accommodation coefficient specifying the fraction of molecules reflected diffusely while the rest is reflected specularly. Due to its simplicity, this model is widely used both in simulations and for characterizing experimental data (see the reviews of Agrawal and Prabhu [55] and Cao *et al.* [37]). Note that Knudsen [25] interpreted his experimental results on radiometric forces by invoking a difference in accommodation coefficients on opposite sides of a vane. In this paper our focus was on the impact of walls with low accommodation upon

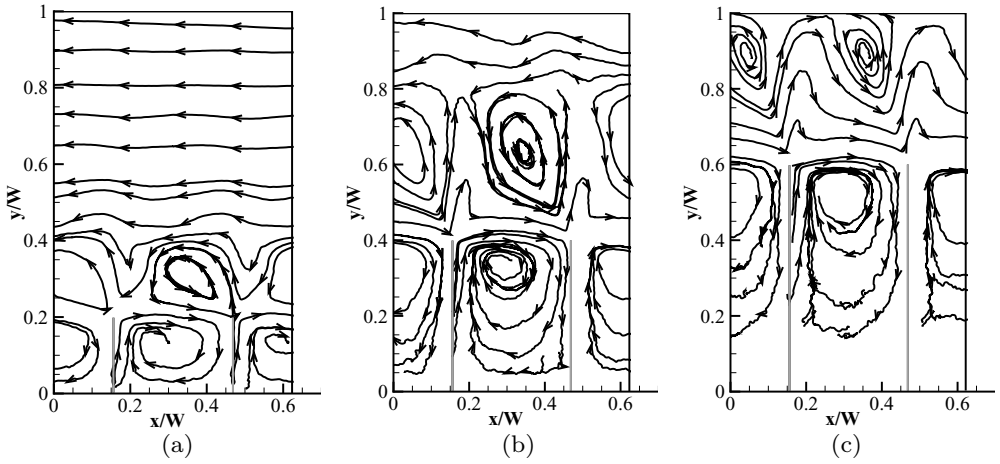

FIG. 10. Velocity field at Kn = 3 and $W/L = 3.2$ for (a) $H/W = 0.2$, (b) $H/W = 0.4$, and (c) $H/W = 0.6$.

reflection of molecules and we therefore considered the extreme cases of ideal diffuse and ideal specular reflection. Although most surfaces have accommodation coefficients not too far away from 1, we stress that this is not merely an academic exercise. Low values in the range of 0.1–0.4 have been obtained both experimentally and numerically for certain gas-surface combinations, opening the possibility of a customized patterning of surface reflectivities.

Specular reflection is often considered to be detrimental to thermally induced rarefied gas flows. Here we not only have shown that a specularly reflecting surface shapes the temperature profile in an essential way, but also argued that it contributes directly to flow over edges where a normal temperature gradient occurs. In particular, we have studied a Knudsen pump inspired by the Crookes radiometer with vanes placed into an inhomogeneous temperature field. Contrary to the Crookes

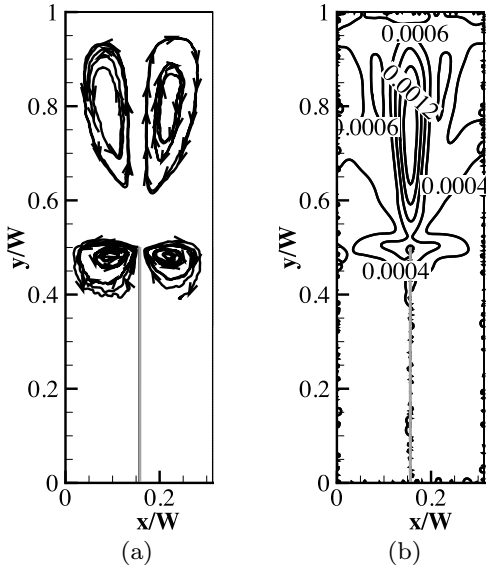

FIG. 11. Fully diffuse vane array at Kn = 3, $H/W = 0.5$, and $W/L = 3.2$ for (a) streamlines and (b) isolines of the local Mach number. The temperature ratio between the sidewall and vanes is again $T_2/T_1 = 2$.

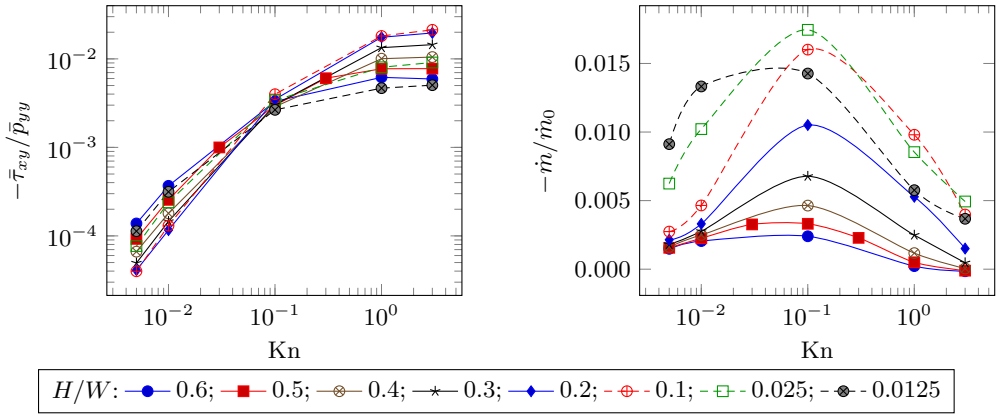

FIG. 12. Shown on the left is the normalized force density $\bar{\tau}_{xy}/p_{yy}$ on the channel sidewall as a function of Kn for variable H/W. On the right is the normalized mass flow along the channel as a function of Kn for variable H/W (lines are merely guides for the eye).

radiometer, where the temperature gradient comes about by selectively heating one side of each vane (thus giving opposite sides different temperatures), in the present case the temperature field is shaped in an essential way by a specularly reflecting boundary on one side of the vane. The origin of the observed forces on the vanes and their dependence on the Knudsen number was discussed based on a simple argument by Einstein. As was pointed out already by Aoki *et al.* [51], at low Kn the corresponding flow across the vanes is essentially of the same kind as thermal creep flow along a wall with a tangential temperature gradient or thermal edge flow at a vane with a different temperature than its surroundings. As such, at low Kn it can be interpreted as a pure boundary effect, needed to reconcile the continuum field equations with the discontinuous phase space density at a wall. For the similar flow across the vane of a Crookes radiometer Taguchi and Aoki [29,46] coined the term radiometric flow.

Utilizing specular walls in a Knudsen pump offers several advantages. In the present geometry, apart from shaping the temperature profile in an essential way, the specular walls do not themselves partake in the exchange of energy between the hot and cold sections of the domain. This may be advantageous for the efficiency of the pump. Furthermore, due to the large velocity slip at walls with low accommodation coefficients, the inclusion of such walls in a Knudsen pump potentially results in larger flow velocities due to reduced viscous dissipation in the system. However, in the current setup with vanes normal to the flow direction this will be a small effect, but should boost the performance in systems with slanted sidewalls such as ratchets [15,18,19].

ACKNOWLEDGMENTS

All numerical calculations were done on the Lichtenberg high performance computer at the TU Darmstadt. E.R. is indebted to the Deutscher Akademischer Austauschdienst for financial support of his visit to Darmstadt. The authors would like to thank Tom Scanlon from the University of Strathclyde for providing access to the dsmcFoamStrath solver. Finally, we express our gratitude to Craig White from the University of Glasgow for sharing his expertise in dsmcFoamStrath.

APPENDIX A: FLOW FIELD AT LARGE Kn AND VARIATION OF H/W

In Sec. V we observed that for large Knudsen numbers the net mass flow direction can be opposite to the flow direction at small Kn. We identified the appearance of edge vortices as the cause for this flow reversal. In order to further investigate the influence of the edge vortex on the flow, we plot streamlines at Kn $= 3$ for various values of H/W in Fig. 10. Note that in each case the vortex

occupies roughly equal amounts of the channel such that it influences the net flow strongest for small gaps between vane and channel wall. Indeed, at Kn = 3, the net flow is in the opposite direction to the direction of force on the sidewalls only for $H/W \gtrsim 0.4$.

TABLE I. Numerical results.

Kn	H/W	$-\bar{\tau}_{xy}/p_0$	$\frac{\sigma(\bar{\tau}_{xy})}{\lvert\bar{\tau}_{xy}\rvert}$	$\bar{p}_{yy}/p_0$	$\frac{\sigma(\bar{p}_{yy})}{\lvert\bar{p}_{yy}\rvert}$	$-\dot{m}/\dot{m}_0$	$\frac{\sigma(\dot{m})}{\lvert\dot{m}\rvert}$	$\bar{q}_y/p_0c_0$	$\frac{\sigma(\bar{q}_y)}{\lvert\bar{q}_y\rvert}$
0.005	0.0125	1.95×10^{-4}	3.3×10^{-2}	1.72	2.5×10^{-3}	9.12×10^{-3}	9.5×10^{-3}	1.37×10^{-2}	1.4×10^{-2}
0.005	0.025	1.28×10^{-4}	9.5×10^{-3}	1.66	2.3×10^{-3}	6.24×10^{-3}	9.8×10^{-3}	1.60×10^{-2}	1.3×10^{-2}
0.005	0.1	6.19×10^{-5}	3.6×10^{-2}	1.55	1.4×10^{-3}	2.74×10^{-3}	2.8×10^{-2}	2.01×10^{-2}	7.7×10^{-3}
0.005	0.2	6.05×10^{-5}	1.9×10^{-2}	1.48	1.1×10^{-3}	2.14×10^{-3}	2.7×10^{-2}	2.31×10^{-2}	6.3×10^{-3}
0.005	0.3	6.99×10^{-5}	8.5×10^{-2}	1.41	7.7×10^{-4}	1.80×10^{-3}	9.3×10^{-3}	2.61×10^{-2}	5.3×10^{-3}
0.005	0.4	9.01×10^{-5}	4.2×10^{-2}	1.36	6.3×10^{-4}	1.62×10^{-3}	9.9×10^{-3}	2.95×10^{-2}	3.9×10^{-3}
0.005	0.5	1.21×10^{-4}	4.0×10^{-2}	1.31	3.1×10^{-4}	1.56×10^{-3}	8.7×10^{-3}	3.38×10^{-2}	2.1×10^{-3}
0.005	0.6	1.74×10^{-4}	1.3×10^{-2}	1.26	3.3×10^{-4}	1.49×10^{-3}	9.6×10^{-3}	3.97×10^{-2}	1.7×10^{-3}
0.01	0.0125	5.59×10^{-4}	7.9×10^{-3}	1.78	1.4×10^{-3}	1.33×10^{-2}	6.5×10^{-3}	2.16×10^{-2}	7.6×10^{-3}
0.01	0.025	4.08×10^{-4}	5.7×10^{-4}	1.70	1.3×10^{-3}	1.02×10^{-2}	6.1×10^{-3}	2.75×10^{-2}	7.4×10^{-3}
0.01	0.1	2.05×10^{-4}	1.2×10^{-2}	1.57	9.5×10^{-4}	4.65×10^{-3}	1.5×10^{-2}	3.73×10^{-2}	4.5×10^{-3}
0.01	0.2	1.73×10^{-4}	6.0×10^{-2}	1.49	1.2×10^{-3}	3.30×10^{-3}	5.2×10^{-3}	4.37×10^{-2}	5.8×10^{-3}
0.01	0.3	2.08×10^{-4}	2.3×10^{-2}	1.42	5.9×10^{-4}	2.77×10^{-3}	1.1×10^{-2}	4.92×10^{-2}	3.2×10^{-3}
0.01	0.4	2.46×10^{-4}	2.9×10^{-2}	1.37	2.8×10^{-4}	2.50×10^{-3}	6.3×10^{-3}	5.53×10^{-2}	1.7×10^{-3}
0.01	0.5	3.36×10^{-4}	2.6×10^{-2}	1.32	1.6×10^{-4}	2.25×10^{-3}	4.8×10^{-3}	6.30×10^{-2}	1.2×10^{-3}
0.01	0.6	4.67×10^{-4}	6.7×10^{-3}	1.27	2.1×10^{-4}	2.05×10^{-3}	6.2×10^{-3}	7.31×10^{-2}	1.3×10^{-3}
0.03	0.5	1.33×10^{-3}	2.7×10^{-3}	1.33	3.3×10^{-5}	3.26×10^{-3}	7.1×10^{-4}	1.58×10^{-1}	1.2×10^{-4}
0.1	0.0125	5.14×10^{-3}	2.5×10^{-3}	1.94	1.5×10^{-4}	1.43×10^{-2}	1.3×10^{-3}	4.29×10^{-2}	2.0×10^{-3}
0.1	0.025	6.40×10^{-3}	1.3×10^{-3}	1.89	1.3×10^{-4}	1.75×10^{-2}	6.3×10^{-4}	7.61×10^{-2}	1.4×10^{-3}
0.1	0.05	7.00×10^{-3}	9.3×10^{-4}	1.81	1.1×10^{-4}	1.83×10^{-2}	5.0×10^{-4}	1.24×10^{-1}	6.6×10^{-4}
0.1	0.1	6.77×10^{-3}	1.1×10^{-3}	1.70	1.1×10^{-4}	1.60×10^{-2}	3.5×10^{-4}	1.83×10^{-1}	3.1×10^{-4}
0.1	0.2	5.48×10^{-3}	7.4×10^{-4}	1.57	4.7×10^{-5}	1.05×10^{-2}	5.7×10^{-4}	2.46×10^{-1}	9.5×10^{-5}
0.1	0.3	4.52×10^{-3}	1.8×10^{-3}	1.49	2.5×10^{-5}	6.77×10^{-3}	4.3×10^{-4}	2.85×10^{-1}	1.1×10^{-4}
0.1	0.4	4.11×10^{-3}	2.0×10^{-3}	1.43	3.6×10^{-5}	4.64×10^{-3}	6.0×10^{-4}	3.17×10^{-1}	7.2×10^{-5}
0.1	0.5	4.10×10^{-3}	3.0×10^{-3}	1.38	1.5×10^{-5}	3.31×10^{-3}	1.2×10^{-3}	3.46×10^{-1}	5.9×10^{-5}
0.1	0.6	4.41×10^{-3}	2.3×10^{-3}	1.33	2.3×10^{-5}	2.40×10^{-3}	2.2×10^{-4}	3.77×10^{-1}	1.9×10^{-5}
0.3	0.5	8.68×10^{-3}	1.6×10^{-3}	1.44	2.6×10^{-5}	2.28×10^{-3}	8.5×10^{-4}	5.23×10^{-1}	1.6×10^{-5}
1	0.0125	9.19×10^{-3}	8.5×10^{-4}	1.97	6.2×10^{-5}	5.76×10^{-3}	3.5×10^{-3}	4.58×10^{-2}	2.2×10^{-3}
1	0.025	1.56×10^{-2}	3.6×10^{-4}	1.94	7.3×10^{-5}	8.53×10^{-3}	2.6×10^{-3}	8.70×10^{-2}	1.0×10^{-3}
1	0.1	3.26×10^{-2}	6.0×10^{-4}	1.80	3.5×10^{-5}	9.80×10^{-3}	1.9×10^{-3}	2.69×10^{-1}	2.7×10^{-4}
1	0.2	2.94×10^{-2}	2.8×10^{-4}	1.67	4.7×10^{-5}	5.28×10^{-3}	1.2×10^{-3}	4.18×10^{-1}	9.3×10^{-5}
1	0.3	2.13×10^{-2}	8.1×10^{-4}	1.59	2.6×10^{-5}	2.48×10^{-3}	1.1×10^{-3}	5.14×10^{-1}	5.9×10^{-5}
1	0.4	1.53×10^{-2}	9.1×10^{-4}	1.53	2.1×10^{-5}	1.17×10^{-3}	3.6×10^{-3}	5.81×10^{-1}	4.9×10^{-5}
1	0.5	1.14×10^{-2}	1.3×10^{-3}	1.48	1.8×10^{-5}	5.03×10^{-4}	2.7×10^{-2}	6.30×10^{-1}	2.3×10^{-5}
1	0.6	8.90×10^{-3}	2.2×10^{-3}	1.44	2.1×10^{-5}	2.23×10^{-4}	6.9×10^{-2}	6.69×10^{-1}	7.4×10^{-6}
3	0.0125	9.93×10^{-3}	3.8×10^{-4}	1.97	7.4×10^{-5}	3.67×10^{-3}	3.2×10^{-3}	4.60×10^{-2}	2.2×10^{-3}
3	0.025	1.77×10^{-2}	6.7×10^{-4}	1.94	5.8×10^{-5}	4.94×10^{-3}	9.0×10^{-4}	8.79×10^{-2}	8.3×10^{-4}
3	0.1	3.83×10^{-2}	2.9×10^{-4}	1.80	5.1×10^{-5}	3.98×10^{-3}	9.0×10^{-4}	2.81×10^{-1}	1.4×10^{-4}
3	0.2	3.29×10^{-2}	2.9×10^{-4}	1.68	2.6×10^{-5}	1.50×10^{-3}	7.0×10^{-3}	4.48×10^{-1}	4.9×10^{-5}
3	0.3	2.31×10^{-2}	6.9×10^{-4}	1.60	2.2×10^{-5}	4.69×10^{-4}	6.5×10^{-3}	5.54×10^{-1}	1.3×10^{-5}
3	0.4	1.61×10^{-2}	8.1×10^{-4}	1.54	1.1×10^{-5}	4.82×10^{-5}	2.6×10^{-1}	6.25×10^{-1}	3.4×10^{-5}
3	0.5	1.16×10^{-2}	1.3×10^{-3}	1.49	2.8×10^{-5}	-1.07×10^{-4}	1.0×10^{-2}	6.74×10^{-1}	3.1×10^{-5}
3	0.6	8.62×10^{-3}	1.5×10^{-3}	1.45	9.4×10^{-6}	-1.52×10^{-4}	2.7×10^{-2}	7.09×10^{-1}	2.7×10^{-5}
10	0.5	1.15×10^{-2}	1.3×10^{-3}	1.50	2.2×10^{-5}	-2.59×10^{-4}	8.2×10^{-2}	6.95×10^{-1}	7.4×10^{-6}

Note that even though the vortex appears on the specular side, it is not a feature exclusive to this boundary condition. When both sides of the vane have the same temperature and are fully diffuse, a symmetric flow pattern with two counterrotating vortices appears above the vane (see Fig. 11). Additionally, two smaller vortices appear on both sides of the vane. Note that at the edge the maximum velocity is parallel to the vane in the main vortices, while it is perpendicular to the vane in the two smaller ones.

The forces and flow rates occurring for half-specular, half-diffuse vanes occupying different fractions of the channel are investigated in Fig. 12. The left panel in this figure shows the ratio between the tangential and the normal force on the sidewall for various vane heights as a function of Kn. As can be seen, the curves all follow the general pattern observed in Fig. 6, although the magnitudes may vary. Similarly, the normalized mass flow shown in the right part of Fig. 12 shows a similar dependence on Kn as in Fig. 9 for all values of H/W. Note, however, that for smaller vanes a significantly larger mass flow can be reached than for the base case $H/W = 0.5$ considered in the main text. This is most likely due to the larger space between vanes and sidewalls. Also note that a mass flow in the positive x direction is only observed for large Kn and large vanes, when the edge vortex discussed above in Fig. 10 occupies the whole width of the channel.

APPENDIX B: TABULATED NUMERICAL RESULTS

In Table I we list numerical results for area-averaged and normalized forces and heat flows on the sidewall ($\bar{\tau}_{xy}$, $\bar{p}_{yy}$, and $\bar{q}_y$) and mass flow along the channel $\dot{m}$. The relative error $\sigma(X)/|X|$ of a quantity X is estimated via the standard deviation from (at least three) consecutive runs. The heat flux at position $\mathbf{r}$ was defined as $\mathbf{q}(\mathbf{r}) = (m/2)\int(\mathbf{c}-\mathbf{u})(\mathbf{c}-\mathbf{u})^2 f(r,c)d^3c$. All results are for $W/L = 3.2$.

[1] H. Struchtrup, *Macroscopic Transport Equations for Rarefied Gas Flows* (Springer, Berlin, 2005).

[2] Y. Sone, *Molecular Gas Dynamics: Theory, Techniques, and Applications* (Birkhäuser, Boston, 2007).

[3] L. D. Landau and E. M. Lifschitz, *Physikalische Kinetik* (Akademie-Verlag, Berlin, 1983).

[4] F. Reif, *Fundamentals of Statistical and Thermal Physics* (McGraw-Hill, New York, 1965).

[5] J. Tyndall, On the action of rays of high refrangibility upon gaseous matter, Philos. Trans. R. Soc. London **160**, 333 (1870).

[6] E. J. Davis and G. Schweiger, *The Airborne Microparticle: Its Physics, Chemistry, Optics, and Transport Phenomena* (Springer, Berlin, 2002).

[7] W. Crookes, Improvement in apparatus for indicating the intensity of radiation, U.S. Patent No. 182172 (12 September 1876).

[8] O. Reynolds, On certain dimensional properties of matter in the gaseous state, Philos. Trans. R. Soc. London **170**, 727 (1879).

[9] J. C. Maxwell, On stresses in rarified gases arising from inequalities of temperature, Philos. Trans. R. Soc. London **170**, 231 (1879).

[10] M. Knudsen, Thermischer Molekulardruck der Gase in Röhren, Ann. Phys. (Leipzig) **338**, 1435 (1910).

[11] Y. Sone, Y. Waniguchi, and K. Aoki, One-way flow of a rarefied gas induced in a channel with a periodic temperature distribution, Phys. Fluids **8**, 2227 (1996).

[12] M. Young, Y. L. Han, E. P. Muntz, G. Shiflett, A. Ketsdever, and A. Green, in *Proceedings of the 23rd International Symposium on Rarefied Gas Dynamics*, edited by A. D. Ketsdever and E. P. Muntz, AIP Conf. Proc. No. 663 (AIP, New York, 2003), p. 743.

[13] S. An, N. K. Gupta, and Y. B. Gianchandani, A Si-micromachined 162-stage two-part Knudsen pump for on-chip vacuum, J. Microelectromech. Syst. **23**, 406 (2014).

[14] H. Sugimoto and Y. Sone, in *Proceedings of the 24th International Symposium on Rarefied Gas Dynamics*, edited by M. Capitelli, AIP Conf. Proc. No. 762 (AIP, New York, 2005), p. 168.
[15] A. A. Donkov, S. Tiwari, T. Liang, S. Hardt, A. Klar, and W. Ye, Momentum and mass fluxes in a gas confined between periodically structured surfaces at different temperatures, Phys. Rev. E **84**, 016304 (2011).
[16] A. Würger, Leidenfrost Gas Ratchets Driven by Thermal Creep, Phys. Rev. Lett. **107**, 164502 (2011).
[17] J. Chen, L. Baldas, and S. Colin, Numerical study of thermal creep flow between two ratchet surfaces, Vacuum **109**, 294 (2014).
[18] J. Chen, S. K. Stefanov, L. Baldas, and S. Colin, Analysis of flow induced by temperature fields in ratchet-like microchannels by direct simulation Monte Carlo, Int. J. Heat Mass Transfer **99**, 672 (2016).
[19] R. Wang, X. Xu, K. Xu, and T. Qian, Onsager's cross coupling effects in gas flows confined to micro-channels, Phys. Rev. Fluids **1**, 044102 (2016).
[20] W. H. Westphal, Messungen am Radiometer II, Z. Phys. **1**, 431 (1920).
[21] A. Einstein, Zur Theorie der Radiometerkräfte, Z. Phys. **27**, 1 (1924).
[22] G. Hettner, Zur Theorie des Radiometers, Z. Phys. **27**, 12 (1924).
[23] T. Sexl, Zur Theorie der Radiometerwirkungen II, Ann. Phys. (Leipzig) **386**, 800 (1926).
[24] P. S. Epstein, Zur Theorie des Radiometers, Z. Phys. **54**, 537 (1929).
[25] M. Knudsen, Radiometerdruck und Akkommodationskoeffizient, Ann. Phys. (Leipzig) **398**, 129 (1930).
[26] H. Martin, *Proceedings of the 14th International Heat Transfer Conference* (American Society of Mechanical Engineers, Washington, DC, 2010), p. 111.
[27] M. Yang and M. Ripoll, A self-propelled thermophoretic microgear, Soft Matter **10**, 1006 (2014).
[28] D. Wolfe, A. Larraza, and A. Garcia, A horizontal vane radiometer: Experiment, theory, and simulation, Phys. Fluids **28**, 037103 (2016).
[29] S. Taguchi and K. Aoki, Motion of an array of plates in a rarefied gas caused by radiometric force, Phys. Rev. E **91**, 063007 (2015).
[30] C. D. F. Honig and W. A. Ducker, Effect of molecularly-thin films on lubrication forces and accommodation coefficients in air, J. Phys. Chem. C **114**, 20114 (2010).
[31] D. Seo and W. A. Ducker, *In Situ* Control of Gas Flow by Modification of Gas-Solid Interactions, Phys. Rev. Lett. **111**, 174502 (2013).
[32] D. Seo and W. A. Ducker, Erratum: *In Situ* Control of Gas Flow by Modification of Gas-Solid Interactions [Phys. Rev. Lett. **111**, 174502 (2013)], Phys. Rev. Lett. **112**, 159904(E) (2014).
[33] D. Seo and W. A. Ducker, Effect of gas species on gas–monolayer interactions: Tangential momentum accommodation, J. Phys. Chem. C **118**, 20275 (2014).
[34] N. Miyoshi, K. Osuka, I. Kinefuchi, S. Takagi, and Y. Matsumoto, Molecular beam study of the scattering behavior of water molecules from a graphite surface, J. Phys. Chem. A **118**, 4611 (2014).
[35] W. Lei and D. R. McKenzie, Enhanced water vapor flow in silica microchannels: The effect of adsorbed water on tangential momentum accommodation, J. Phys. Chem. C **119**, 22072 (2015).
[36] D. Blanchard and P. Ligrani, Slip and accommodation coefficients from rarefaction and roughness in rotating microscale disk flows, Phys. Fluids **19**, 063602 (2007).
[37] B.-Y. Cao, J. Sun, M. Chen, and Z.-Y. Guo, Molecular momentum transport at fluid-solid interfaces in MEMS/NEMS: A review, Int. J. Mol. Sci. **10**, 4638 (2009).
[38] S. Hardt, S. Tiwari, and A. Klar, Momentum transfer to nanoobjects between isothermal parallel plates, Microfluid. Nanofluid. **6**, 489 (2009).
[39] G. A. Bird, *Molecular Gas Dynamics and the Direct Simulation of Gas Flows* (Clarendon, Oxford, 1994).
[40] T. J. Scanlon, E. Roohi, C. White, M. Darbandi, and J. M. Reese, An open source, parallel DSMC code for rarefied gas flows in arbitrary geometries, Comput. Fluids **39**, 2078 (2010).
[41] R. C. Palharini, C. White, T. J. Scanlon, R. E. Brown, M. K. Borg, and J. M. Reese, Benchmark numerical simulations of rarefied non-reacting gas flows using an open-source DSMC code, Comput. Fluids **120**, 140 (2015).
[42] T. J. Scanlon, C. White, M. K. Borg, R. C. Palharini, E. Farbar, I. D. Boyd, J. M. Reese, and R. E. Brown, Open-source direct simulation Monte Carlo chemistry modeling for hypersonic flows, AIAA J. **53**, 1670 (2015).

[43] H. G. Weller, G. Tabor, H. Jasak, and C. Fureby, A tensorial approach to computational continuum mechanics using object-oriented techniques, Comput. Phys. **12**, 620 (1998).
[44] A. O. Ahmad, Advances in an open-source direct simulation Monte Carlo technique for hypersonic rarefied gas flows, Ph.D. thesis, University of Strathclyde, 2013.
[45] C. Borgnakke and P. S. Larsen, Statistical collision model for Monte Carlo simulation of polyatomic gas mixture, J. Comput. Phys. **18**, 405 (1975).
[46] S. Taguchi and K. Aoki, Rarefied gas flow around a sharp edge induced by a temperature field, J. Fluid Mech. **694**, 191 (2012).
[47] N. Selden, C. Ngalande, S. Gimelshein, E. P. Muntz, A. Alexeenko, and A. Ketsdever, Area and edge effects in radiometric forces, Phys. Rev. E **79**, 041201 (2009).
[48] L. Waldmann, Über die Kraft eines inhomogenen Gases auf kleine suspendierte Kugeln, Z. Naturforsch. Teil A **14**, 589 (1959).
[49] S. P. Bakanov and B. V. Derjaguin, The motion of a small particle in a non-uniform gas mixture, Discuss. Faraday Soc. **30**, 130 (1960).
[50] Y. Sone and M. Yoshimoto, Demonstration of a rarefied gas flow induced near the edge of a uniformly heated plate, Phys. Fluids **9**, 3530 (1997).
[51] K. Aoki, Y. Sone, and N. Masukawa, A rarefied gas flow induced by a temperature field, Rarefied Gas Dyn. **1**, 35 (1995).
[52] D. A. Lockerby, J. M. Reese, D. R. Emerson, and R. W. Barber, Velocity boundary condition at solid walls in rarefied gas calculations, Phys. Rev. E **70**, 017303 (2004).
[53] M. Scandurra, F. Iacopetti, and P. Colona, Gas kinetic forces on thin plates in the presence of thermal gradients, Phys. Rev. E **75**, 026308 (2007).
[54] A. Ventura, N. Gimelshein, S. Gimelshein, and A. Ketsdever, Effect of vane thickness on radiometric force, J. Fluid Mech. **735**, 684 (2013).
[55] A. Agrawal and S. V. Prabhu, Survey on measurement of tangential momentum accommodation coefficient, J. Vac. Sci. Technol. A **26**, 634 (2008).